Magnetic coupling of ferromagnetic stripe arrays: Analytical model for the α-β-phase coexistence regime of MnAs/GaAs(001)

R. Engel-Herbert*
Materials Department, University of California—Santa Barbara, Santa Barbara, California 93106-5050, USA

T. Hesjedal
Magnetic Materials Laboratory, University of Waterloo, Waterloo, Ontario, Canada N2L 3G1

(Received 3 June 2008; revised manuscript received 10 November 2008; published 18 December 2008)

We investigate the temperature-dependent hysteresis of the stripe state of MnAs thin films on GaAs(001) in the phase coexistence regime. The underlying magnetic domain structure is described employing an analytic model for stripe arrays with perpendicular anisotropy. In the framework of this model the magnetic properties of the MnAs stripe array can be unraveled as a combined effect of magnetostatic coupling of neighboring ferromagnetic stripes and the tendency to form antiparallel magnetic domains within the individual ferromagnetic stripes. The detailed analysis reveals the balance of demagnetization energy and domain-wall energy for the domain structure. It is capable to quantitatively predict the temperature dependency of the coercive field of MnAs thin films on GaAs(001) in the phase coexistence regime. Further, the analytic model allows for an understanding of the unusual magnetic reversal properties as a consequence of the temperature-driven geometrical variations in the stripe array. Here, it is the energy difference of the single and the multidomain states associated with the geometrical variations, which is the driving factor, rather than the temperature dependence of the magnetic properties themselves. Although the stripe array of MnAs thin films can be in an interstripe as well as in an intrastripe coupling state, the magnetization reversal is entirely determined by interstripe coupling.

DOI: 10.1103/PhysRevB.78.235309 PACS number(s): 75.60.−d, 75.75.+a, 75.10.−b

I. INTRODUCTION

The magnetic properties of artificial and self-organized magnetic nanostructures are of prime importance for their future use in magnetic storage and logic technologies.[1,2] As the integration density of memory bits is increasing rapidly, the magnetostatic coupling between magnetic nanostructures, such as dots and wires, is becoming relevant.[3–5] The study of the magnetostatic coupling phenomena[6] in arrays of magnetic nanostructures is crucial as it determines the magnetization reversal of the single nanostructure as well as that of the ensemble.[7]

Manganese arsenide (MnAs) films on GaAs(001) exhibit remarkable phenomena driven by the epitaxial constraints imposed by the substrate. Many of these phenomena have been the subject of intense studies and are summarized in Ref. 8. In the temperature interval of 10–40 °C two MnAs phases coexist: the ferromagnetic α phase and the nonferromagnetic β phase.[9] Both phases are arranged in a periodic stripe structure due to the anisotropic strain state imposed by the substrate. The period of the stripe structure depends linearly on the film thickness, whereas the widths of MnAs wires in its respective phase only depend on temperature. With increasing temperature the widths of the β-MnAs stripes increase at the cost of the widths of the ferromagnetic α-MnAs stripes.

The underlying domain structure of this coupled array of ferromagnetic stripes was already subject to extensive investigations, both experimentally and by means of micromagnetic simulations.[10,11] The treatment of the problem turned out to be rather complicated due to the variety of different domain structures that are of comparable energy within an isolated magnetic wire.[12] The resulting complex micromagnetic domain structures within the individual stripes usually exhibit a number of metastable states. The influence of temperature—and thus geometrical variation in the stripe structure—was experimentally verified by x-ray magnetic circular dichroism photoemission electron microscopy for the remanent state of MnAs/GaAs(001).[13] For film thicknesses ranging from 120 up to 500 nm, two coupling regimes were found. For lower temperatures and thus stronger magnetic coupling between the ferromagnetic stripes, domains extending across several stripes are favored. For higher temperatures the magnetic coupling breaks down, thus leading to a domain structure favoring the demagnetization within the individual stripes.

The magnetization reversal mechanism of thicker MnAs films on GaAs(001) (115–300 nm) (Ref. 14) is mainly governed by the formation of magnetic flux closure patterns in the basal plane (easy plane).[10,11] Thus, the interstripe coupling only plays a role for very small ferromagnetic stripe separations at lower temperatures within the stripe coexistence regime. For thinner MnAs films the tendency to form flux-closure patterns in the depth of the film is strongly suppressed, and one can expect that the magnetostatic coupling across the wires plays a dominant role.

In this paper, the investigation of the temperature-dependent hysteresis of MnAs/GaAs(001) in the phase coexistence regime is extended toward thinner films. Recently it has been reported that MnAs thin films show a nonmonotonic temperature dependency of the coercive field.[15] However, no conclusive explanation of the unusual behavior of the coercivity was given. We will use an analytic model for stripe arrays with perpendicular anisotropy[16] and employ an energy minimization method used for magnetic multilayer structures.[17] These allow us to calculate the energy of the

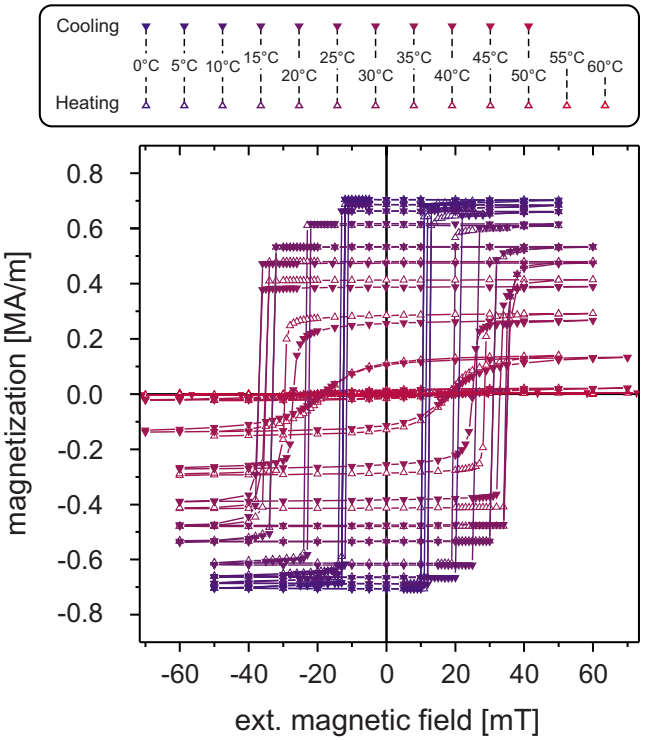

FIG. 1. (Color online) Magnetic hysteresis curves of a 60-nm-thick MnAs/GaAs(001) film at different temperatures in the phase coexistence regime measured for a heating cycle (△) and a cooling cycle (▼).

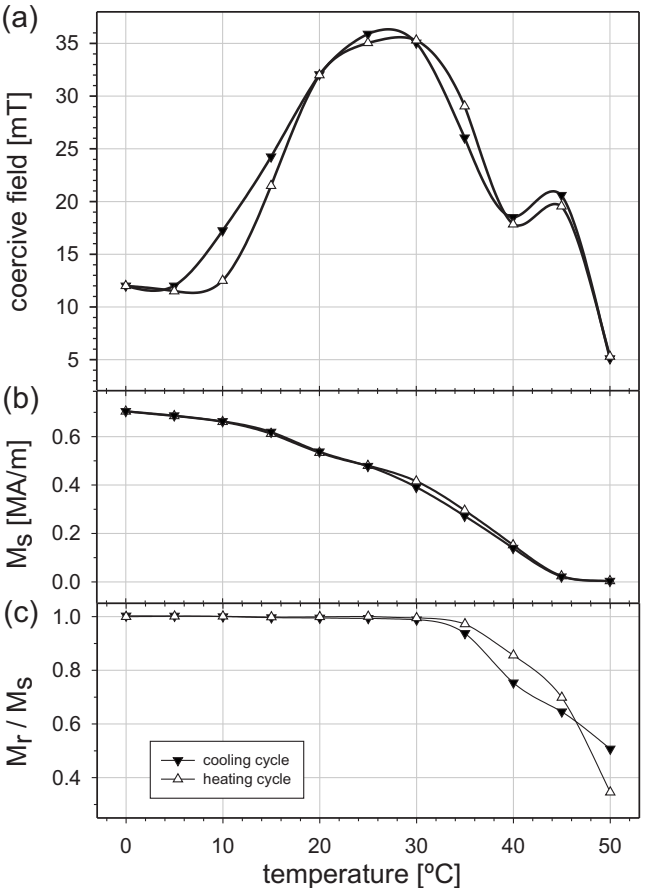

FIG. 2. Magnetic quantities of a 60-nm-thick MnAs/GaAs(001) film deduced from magnetic hysteresis curves shown in Fig. 1: temperature dependency of (a) coercive field, (b) saturation magnetization at maximum applied field, and (c) ratio of remanent and saturation magnetizations M_r and M_s.

domain structure depending on the arrangement of the MnAs phases. It will be shown that the energies associated with the stripe array and its underlying domain structure are capable to render the characteristics of the measured hysteresis curves. The peculiar temperature-dependent features of the hysteresis curve will be explained solely by the gradual geometrical change in the stripe structure in the phase coexistence regime and the bulk magnetic properties of the ferromagnetic MnAs phase.

The paper is organized as follows. In Sec. II we summarize the experimental findings of MnAs thin film magnetization curves presented in Ref. 15. In Sec. III the analytical domain model is introduced. In Sec. IV the results from the analytical model are discussed and compared with the experimental findings. The conclusions are given in Sec. V.

II. EXPERIMENTAL FINDINGS

The MnAs/GaAs(001) samples under investigation show the following epitaxial relationships: MnAs($\bar{1}100$)∥GaAs(001) and MnAs[0001]∥GaAs[$1\bar{1}0$]; they have their magnetic easy axis (a axis) along MnAs[$11\bar{2}0$] and their hard axis (c axis) along MnAs[0001]. The epitaxial sample growth by the molecular-beam epitaxy (MBE) is described in Refs. 18–21. Hysteresis curves of a 60-nm-thick MnAs film were measured with a superconducting quantum interference device (SQUID) magnetometer, as shown in Refs. 15 and 22. Figure 1 displays a temperature cycle of the magnetic hysteresis curves for an external field applied along the in-plane a axis of MnAs recorded in steps of 5 °C. The temperature interval ranges from 0 to 60 °C for the heating sequence and from 50 to 0 °C for the cooling sequence. The magnetization curves measured for both the heating and cooling sequences are in very good agreement at low and high temperatures. For intermediate temperatures in the phase coexistence region, however, the magnetization values of the cooling sequence are slightly smaller. This indicates a small temperature hysteresis of the α-MnAs phase composition. It is also apparent that for higher temperatures the shape of the magnetic hysteresis curve changes from a rectangular to a rounded shape near the coercive fields. This gradual change in the magnetization around the coercive field indicates that the magnetization reversal is initiated by a rotational reversal rather than instantaneous domain nucleation and subsequent domain-wall movement.

Figure 2 summarizes the temperature trend of the magnetic hysteresis curves. The most prominent feature is the nonmonotonic change in the coercive field with temperature shown in Fig. 2(a). At low temperatures the coercivity increases with increasing temperature, reaches a maximum at around 28 °C, and decreases monotonically with increasing temperature. The coercivity values at 45 °C are not directly following this trend and will be discussed later. The satura-

tion magnetization at high magnetic fields, shown in Fig. 2(b), decreases monotonically with temperature. The main reduction in the saturation magnetization is not due to the temperature-dependent decrease in the magnetic moment but is mainly governed by the nucleation and formation of the β-MnAs phase with zero net magnetic moment. The average width of the β-MnAs stripes increases almost linearly with higher temperature. This is in good agreement with x-ray magnetic circular dichroism photoemission electron microscopy measurements on a 40-nm-thick MnAs film[23] and specular and diffuse x-ray scattering on a 130-nm-thick MnAs film.[24]

The ratio of remanent to saturation magnetization is shown in Fig. 2(c). It remains unity up to temperatures at which the stripe structure exhibits the maximum coercivity. At higher temperature the ratio reduces, which correlates with the rounding of the hysteresis curves.

III. MICROMAGNETIC DOMAIN MODEL

The experimentally observed arrangement of the MnAs phases in the coexistence regime was recently reported employing atomic force microscopy[25] and low electron energy microscopy.[26] Figure 3 shows the model of the stripe array apparent in MnAs/GaAs(001) in the phase coexistence regime (c axis$\equiv$[0001] and a axis$\equiv[11\bar{2}0]$ directions of MnAs). A multistripe structure consisting of an alternating sequence of ferromagnetic α-MnAs stripes of width w_α and β-MnAs stripes of width w_β extends along the x axis (c-axis direction of MnAs). Multiples of this elementary stripe pattern of period p are repetitive along the y axis (a-axis direction of MnAs). The magnetization direction inside the domains is assumed to be exclusively oriented in the y direction. The lengths of domains with magnetization in the $+y$ direction are d_+ and in the $-y$ direction d_-, respectively. Following Ref. 17, domain walls separating antiparallel magnetized domains are assumed to be infinitely thin and freely mobile. It has to be noted that the model simplifies the realistic stripe structure: it only takes into account the average stripe width of the phases. Local deviations, such as narrowing and widening of the stripes or edge dislocations, will be neglected.

In the y direction, the domain magnetization of neighboring stripes is parallel. The domains can couple via magnetostatic interaction and align parallel across the β-MnAs stripes to obtain a minimum magnetostatic energy. This is a valid assumption in the absence of antiferromagnetic interlayer coupling across the β-MnAs stripes.[27] It has to be noted that there is no experimental evidence for long-range antiferromagnetic ordering in β-MnAs.[9] The material separating the ferromagnetic stripes is assumed to have a zero net magnetization and hence no magnetic stray fields.

To derive the total energy associated with the domain structure, a model is employed which was used for perpendicularly magnetized multilayered structures.[17,27] The relevant expression for demagnetization and domain-wall energies has to be adapted for the periodic stripe structure. A detailed derivation of the energy expressions is given elsewhere.[16]

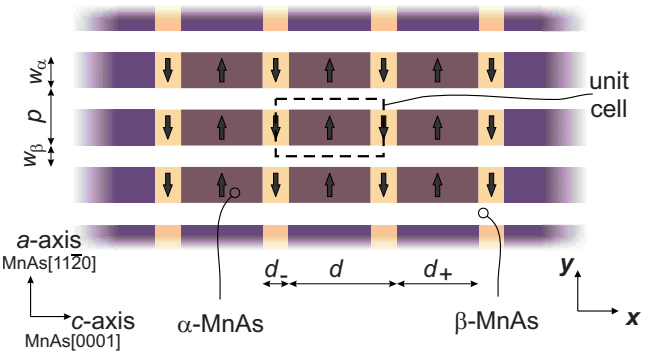

FIG. 3. (Color online) Model of the stripe structure and its magnetic domain arrangement for thin MnAs films of thickness t on GaAs(001).

The two main prerequisites to employ the analytical apparatus are the following: (i) the magnetization is constant within a domain throughout the depth of the film and (ii) the anisotropy is large enough to orient all domains perpendicular to the stripes. The stripe structure of MnAs/GaAs(001) fulfills these requirements in the phase coexistence regime. (i) The squarelike hysteresis and high remanence at low temperatures suggest the absence of domain structures in the depth of the film. Although no minimal film thickness was reported as a lower threshold for the formation of flux closure domains, these multidomain (MD) structures in the depth have been observed for film thicknesses larger than 100 nm.[28] They are energetically disfavored for thinner films. The exchange energy scales with the dimensions and the gain in reducing the demagnetization energy at the expense of exchange energy is not high enough. (ii) The effective easy axis in MnAs/GaAs(001) is lying in the film plane perpendicular to the direction of the stripe axis.[29] The reason is a superposition of the easy-plane character of the magnetocrystalline anisotropy and the shape anisotropy.[30,31] SQUID measurements revealed that the out-of-plane magnetization component is smaller than 1% at remanence.[22] It has to be noted that, with the c axis being the magnetocrystalline hard axis, the only possible domain transition is of Bloch-wall type with the wall surface normal along the c axis (x axis in Fig. 3). As the dimensions of the stripes change with temperature it has to be discussed up to which point prerequisite (ii) is fulfilled.

For the modeling of the MnAs films a platelet containing a periodic distribution of only one magnetization component M_y is assumed; the other two components are zero $M_x=M_z=0$. The unit cell of the domain structure is shown in Fig. 3 along with the geometrical parameters of the stripe array. The period $p=w_\alpha+w_\beta$ in the y direction is given by the width of the ferromagnetic stripes w_α (α-MnAs phase) and the width of the stripes in the β-MnAs phase w_β, separating α-MnAs stripes. The period in the x direction is given by the domain repetition length d as the sum of the domain widths being magnetized in the $+y$ and the $-y$ directions, d_+ and d_-, respectively. The average magnetization m per unit cell can thus be expressed by

$$m = \frac{d_+ - d_-}{d} M_s, \tag{1}$$

where M_s is the saturation magnetization.

The total-energy density ε_{tot} of the domain structure consists of three terms:

$$\varepsilon_{tot} = \varepsilon_{dem} + \varepsilon_{dw} + \varepsilon_{ext}, \tag{2}$$

the demagnetization energy density ε_{dem}, the energy density ε_{dw} associated with the formation of domain walls, and the energy density ε_{ext} due to an externally applied field. All terms are normalized with respect to the maximum magnetostatic energy density $K_d = \mu_0/2M_s^2$. For the demagnetization energy an expression is derived[16] using the Fourier approach for biperiodic magnetization distribution in a platelet.[32] For the unit cell of the periodic domain structure of MnAs (cf. Fig. 3), the demagnetization energy can be written as

$$\varepsilon_{dem} = \frac{4}{p^2}\sum_l{}' \sin^2\left(\pi l \frac{w_\alpha}{p}\right) \times \left[m^2 + \sum_k{}' \frac{16\sin^2[\pi k/2(m+1)]}{\pi^2 k^2}\right] f_{k,l}(a,p,d), \tag{3}$$

with

$$f_{k,l}(a,p,d) = \frac{1}{\tau^2}\left[1 - \frac{\sinh(\tau a)}{\tau a[\cosh(\tau a) + \sinh(\tau a)]}\right],$$

where $\tau = 2\pi\sqrt{(k/d)^2 + (l/p)^2}$ and $a = t/2$ (film thickness t).

The primed sums in Eq. (3) indicate that the terms with index variable zero are excluded. The convergence of the series depends on the geometrical parameters and is discussed in Ref. 16. It has to be noted that the expression for the demagnetization energy is only valid for $w_\alpha < p$; i.e., it is not possible to use this expression to describe the transition of the stripe structure to a continuous film $w_\alpha = p$. For a continuous film, the demagnetization energy approaches zero since divergences or magnetic surface charges are absent.

The second energy term in Eq. (2) associated with the magnetic domain structure is the exchange energy. It is confined to the domain walls since the magnetization is constant inside the domains. The domain transition is of Bloch-wall type where the magnetization rotates out of the plane over the "intermediate" anisotropy axis. The domain-wall energy can be described by

$$\varepsilon_{dw} = \frac{2w_\alpha}{pd}\frac{\gamma}{\mu_0/2M_s^2} = \frac{2w_\alpha}{pd}\delta, \tag{4}$$

where γ is the wall energy per unit area and δ is the Bloch-wall width. Equation (4) takes into account the number of domain walls per repetition length d and the width of the stripes (see Fig. 3). The ratio of the domain-wall energy and the maximum demagnetization energy density is given by δ. The domain-wall energy γ and thus the width δ are given by the exchange stiffness constant A and anisotropy constant K.[33] The origin of the effective easy axis is a superposition of the magnetocrystalline anisotropy and the shape anisotropy. The strong magnetocrystalline anisotropy suppresses the magnetization along the c axis of MnAs (x axis in Fig. 3). The anisotropy of the stripe array of MnAs/GaAs(001) is therefore modeled by the demagnetization factors for rectangular prisms in the limit of infinite extension in one dimension (along the x axis).[34] The demagnetization factor for the effective in-plane easy axis direction (y axis in Fig. 3) is given by

$$N_y = \frac{1}{\pi}\left[\frac{4a^2 - w_\alpha^2}{4aw_\alpha}\ln\left(1 + \left(\frac{w_\alpha}{2a}\right)^2\right) + \frac{w_\alpha}{2a}\ln\left(\frac{w_\alpha}{2a}\right) + 2\arctan\left(\frac{2a}{w_\alpha}\right)\right]. \tag{5}$$

The demagnetization contribution in the x direction can be neglected, as the magnetocrystalline anisotropy suppresses the magnetization in the x direction, thus $N_z = 1 - N_y$. The wall energy per unit area follows[33]

$$\gamma = 4\sqrt{AK} = 4\sqrt{AK_d(1 - 2N_y)}, \tag{6}$$

with K being the effective anisotropy constant, which is expressed by the maximum demagnetization energy density K_d and the demagnetization factors. From Eq. (5) it is apparent that for decreasing stripe shape ratios, the domain-wall energy is not only decreased due to the reduction in cross-sectional area but also additionally due to the monotonic decrease in the demagnetization factors. The case $N_y = N_z = 0.5$ is the limit of the domain model. In the cross section (y-z plane) the stripes become square shaped. The shape anisotropy will not lead to an effective easy axis and the y direction is not energetically preferred anymore. Thus, the model is not applicable anymore [prerequisite (ii) is violated].

The third term that contributes to the total-energy density is the Zeeman term due to an externally applied field H (normalized field h). Assuming that the field is only applied along the $+y$ direction, we obtain

$$\varepsilon_{ext} = \frac{-\mu_0 Hm}{\mu_0/2M_s^2} = -2hm. \tag{7}$$

To find the equilibrium magnetization the total energy is minimized with respect to m,

$$\frac{\partial\varepsilon_{tot}}{\partial m} = 0 \rightarrow h = \frac{4}{w_\alpha p}\sum_l{}' \sin^2\left(\pi l \frac{w_\alpha}{p}\right) \times \left[m + \sum_k{}' \frac{8\sin[\pi k(m+1)]}{\pi^2 k^2}\right] f_{k,l}(a,p,d), \tag{8}$$

and the domain repetition length d,

$$\frac{\partial\varepsilon_{tot}}{\partial d} = 0 \rightarrow d = \sqrt{\frac{2w_\alpha}{p}\frac{\delta}{\partial\varepsilon_{dem}/\partial d}}. \tag{9}$$

IV. DISCUSSION

The calculation procedure is now as follows.[17] For a given magnetization m the field h is calculated using Eq. (8), at which the magnetization has a minimum total energy. The domain repetition length d is numerically determined from Eq. (9), which is implicit in d. The remaining parameters for the calculations are the geometrical dimensions of the stripe

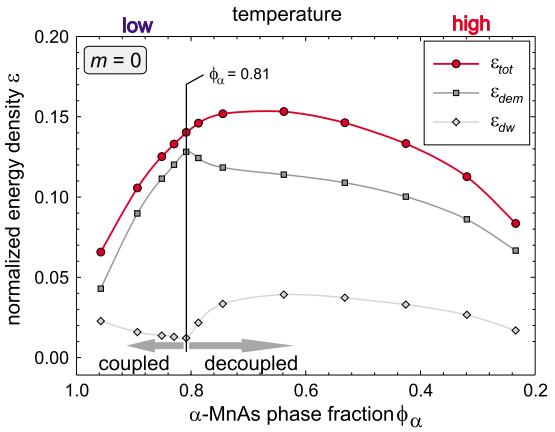

FIG. 4. (Color online) Energy contributions of the stripe array with zero net magnetization for different α-MnAs phase fractions ϕ_α.

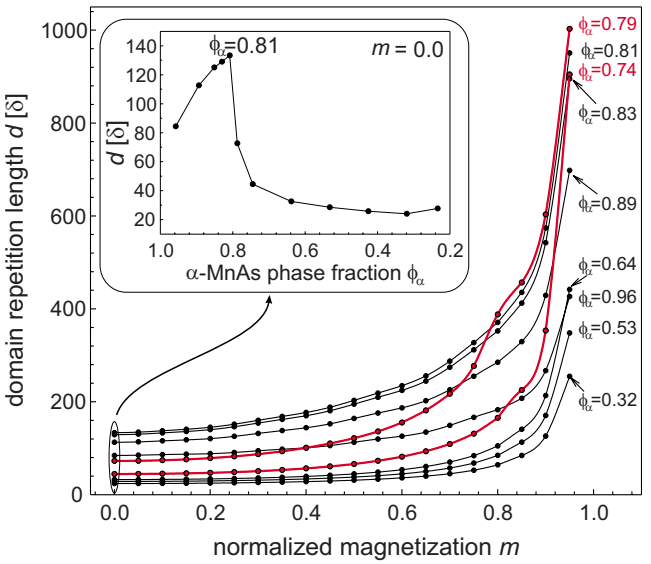

FIG. 5. (Color online) Domain repetition length d as a function of magnetization m for different α-MnAs phase fractions ϕ_α. The inset shows a plot of d in zero applied field as a function of the phase fraction ϕ_α.

structure, the exchange stiffness constant A, and saturation magnetization M_s.

It has been found that the stripe period p scales linearly with the film thickness t $(=2a)$: $p=4.7t$.[8] The calculations were carried out from ferromagnetic stripe widths $w_\alpha=4.5t$ (corresponding to a low temperature) to $w_\alpha=1.1t$ (high temperature). The lower limit of w_α is given by the prerequisite of an easy a axis and the upper limit from the experimentally determined onset of the stripe phase. In the following discussion, a film thickness of $t=60$ nm was chosen in accordance with the experiments (cf. Fig. 1). The saturation magnetization was extracted from the temperature-dependent magnetization curves. According to Figs. 1 and 2(b), $M_s=700$ kA/m at 0 °C. Finally, an exchange stiffness constant of $A=10^{-11}$ J/m was assumed.[28]

A. Results of the micromagnetic model

Numerical calculations of the energy densities were carried out for normalized magnetization values from $m=0$ up to 0.95 in steps of 0.05. First, the results of the micromagnetic modeling will be discussed within its validity limits for a heating cycle in the absence of an externally applied field $(h=0)$. From Eq. (8) it follows that $m=0$, i.e., domain widths d_+ and d_- are equal. For this case the balancing of the demagnetization and domain-wall energies is shown in Fig. 4 as a function of the α-MnAs phase fraction. The α-MnAs phase fraction ϕ_α is defined as the ratio of w_α and p and thus depends on the sample temperature. With decreasing α-MnAs phase fraction (increasing temperature during a heating cycle), the total energy increases up to $\phi_\alpha \approx 0.7$ and decreases again for smaller phase fractions. The underlying demagnetization and domain energies $\varepsilon_{\mathrm{dem}}$ and $\varepsilon_{\mathrm{dw}}$ show a discontinuous dependency on the α-MnAs phase fraction with a transition at $\phi_\alpha=0.81$. This marks the change in the coupling state from interstripe coupling for larger ϕ_α to a decoupled state for smaller ϕ_α.

The trend of the energy terms $\varepsilon_{\mathrm{dem}}$ and $\varepsilon_{\mathrm{dw}}$ with decreasing α-MnAs phase fractions can be understood from Eq. (3) and Eqs. (4)–(6), respectively. Whereas the demagnetization energy density is inversely proportional to the ratio $\phi_\alpha = w_\alpha/p$, the domain-wall energy contribution is proportional to ϕ_α. The increase in demagnetization energy is caused by the boundary condition of the magnetic flux. A continuous normal component across the stripe (along the y direction) is required. Consequently the normal component of the magnetic field is discontinuous. Smaller α-MnAs phase fractions and thus larger stripe separations w_β increase the component of the demagnetization field H_y inside the domains, which causes the increase in demagnetization energy. The origin in the decrease in the domain-wall energy is twofold. For one, a smaller ϕ_α reduces the domain-wall area according to Eq. (4). In addition, the wall energy per unit area also decreases due to a decrease in the effective anisotropy constant K according to Eqs. (5) and (6).

At the α-MnAs phase fraction of $\phi_\alpha=0.81$ this trend is reversed. The energy reduction due to a decrease in domain-wall energy does not sufficiently compensate the increase in demagnetization energy. The discontinuous nature of this transition is caused by a change in the domain repetition length d, calculated from Eq. (9). The change in d with ϕ_α is shown in the inset of Fig. 5. The domain repetition length sharply falls off for $\phi_\alpha<0.81$.

For a further decrease in the α-MnAs phase fraction below $\phi_\alpha=0.7$ the domain-wall and demagnetization energies monotonically decrease. In this regime the domain-wall repetition length d does not drastically change. The reason for the decrease in domain-wall energy is again the reduction in the cross-sectional area of the stripe and decrease in the effective anisotropy constant. The demagnetization energy decreases too as the α stripes decrease in width and occupy lesser volume.

The change in the ratio of two energy contributions is connected to the change in the domain repetition length. Therefore it is mandatory to understand its role in the micromagnetic domain model and how it is affected by the coupling behavior of the domains in the stripe array. The domain

repetition length d represents a measure of the ratio of the two energy terms $\varepsilon_{\mathrm{dem}}$ and $\varepsilon_{\mathrm{dw}}$. The larger the domain repetition length, the smaller the domain-wall energy cost per length compared to the demagnetization energy. In other words, it is energetically favorable to keep the domain repetition length long and thus increase the demagnetization energy per unit cell. The domain arrangement and its associated demagnetization energy influences the domain repetition length in two opposite ways. If neighboring domains with the same magnetization are energetically favorable, d gets large. In the stripe array this can only be accomplished by domains that couple across the stripe separation. If neighboring domains with opposite magnetization are energetically favored, d becomes small. For a fixed α-MnAs phase fraction—and thus domain-wall energy contribution—the domain repetition length can be considered as a direct measure of the nature of the coupling. Larger domain repetition lengths indicate a minimization of the demagnetization energy due to interstripe coupling, whereas smaller domain repetition lengths indicate that each stripe tries to minimize its demagnetization energy individually. In this context, the minimization of the total energy with respect to d, and thus Eq. (9), can be considered as the balancing of these two energies.

For larger phase fractions, the system favors the minimization of the demagnetization energy through parallel domains across the stripe separation instead of antiparallel neighboring domains within the individual stripes. Thus, for zero net magnetization, the α-MnAs phase fraction of $\phi_\alpha = 0.81$ marks the transition from a coupled stripe array for larger α-MnAs phase fractions and a decoupled stripe array for smaller α-MnAs phase fractions.

The transition from the coupled stripe array to a decoupled stripe array is not uniquely determined by the α-MnAs phase fraction but depends on the applied magnetic field too. This is shown in Fig. 5 where the domain repetition length d is plotted as a function of magnetization $m(h)$. Corresponding h values have been omitted in this discussion. In general, it is observed that the domain repetition length increases with increasing magnetization, i.e., increasing difference in the domain widths d_+ and d_-. Stripe arrays with an α-MnAs phase fraction $\phi_\alpha \geq 0.81$ never change their coupling state—they always remain coupled. However, arrays with $\phi_\alpha = 0.79$ and $\phi_\alpha = 0.74$ show a mix of the two different coupling regimes [cf. the highlighted curves (in red) in Fig. 5]. For small magnetization values, the arrays are in the decoupled state and d is comparably small. With increasing magnetization, a disproportionate increase in the domain repetition length is observed for larger magnetization values of $m \approx 0.7-0.9$. For an increasing asymmetry in the width of the domains, the magnetic flux cannot very effectively form closed field lines through the "bottleneck" of the neighboring antiparallel magnetized domain. Instead, it is forced to protrude further away from the stripe. Thus the magnetic field can couple to the parallel domain in the neighboring stripes—the onset of the interstripe coupling regime.

Extending the above discussion to arrays with α-MnAs phase fractions $\phi_\alpha < 0.74$ does not directly allow for a prediction of the coupling state in saturation. Although it was shown that they are decoupled for $m=0$ and do not exhibit a superproportional increase in domain repetition length with applied field, the superproportional increase might be shifted toward larger magnetization values and is overlayed by the general increase in d with m. In Sec. IV B, we will show that the magnetization reversal mechanism is governed by interstripe coupling throughout the entire phase coexistence regime.

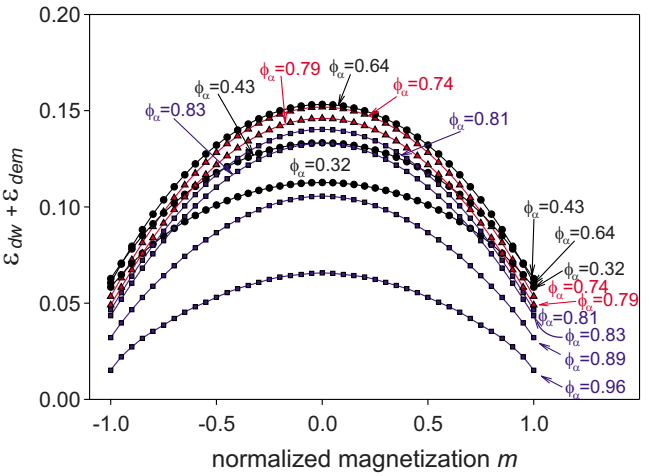

FIG. 6. (Color online) Total energy of the stripe array in the absence of an externally applied field for given α-MnAs phase fractions ϕ_α as a function of the magnetization m.

B. Comparison with experimental results

We will now compare the results of the micromagnetic model with the experimental results discussed in Sec. II. For the following discussion it is necessary to consider two different magnetization states of the stripe array: the single domain (SD) and the MD states. In the SD state, the total energy consists of the Zeeman term $\varepsilon_{\mathrm{ext}}$ and the demagnetization energy $\varepsilon_{\mathrm{dem}}$ and for the MD state, it consists additionally of the domain-wall energy $\varepsilon_{\mathrm{dw}}$.

Figure 6 shows the demagnetization and domain-wall energy densities as functions of the magnetization for different α-MnAs phase fractions. It has to be noted that Eq. (3) can be used to calculate the demagnetization energy density for completely saturated stripe arrays. For $m = \pm 1$, the summands for $k \neq 0$ become zero and the demagnetization energy density is not longer dependent on the domain repetition length d.

The energy of the stripe array (shown in Fig. 6) is a parabolic function of the magnetization and can be expressed by

$$\varepsilon_{\mathrm{tot}}(m) = -(\varepsilon^{\mathrm{MD}} - \varepsilon^{\mathrm{SD}})m^2 - 2hm + \varepsilon^{\mathrm{MD}}, \qquad (10)$$

where $\varepsilon^{\mathrm{MD}}$ and $\varepsilon^{\mathrm{SD}}$ are the energies of the stripe array in the MD state with zero net magnetization and in the SD state at saturation, respectively. Please note that Eq. (10) is not an approximation of Eq. (2). Fitting the data presented in Fig. 6 using a second-order polynomial function revealed excellent agreement with $R^2 > 0.997$.

Independent of the α-MnAs phase fraction, the energy minimum is achieved when the stripe array is in saturation (single domain state). Mathematically it means that the glo-

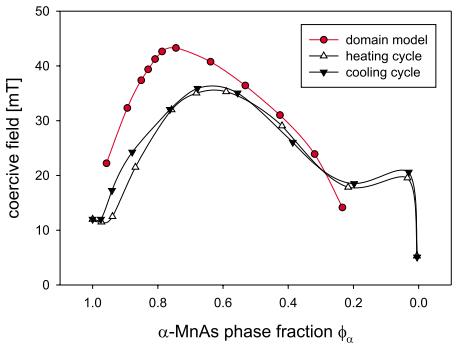

FIG. 7. (Color online) Comparison of the derived switching field for arrays with different stripe shape ratios with experimental data for temperatures in the phase coexistence regime.

bal energy minimum of the system is always the saturated state (single domain state), expressed by the parabolic dependency of the energy as a function of magnetization. Furthermore, Eq. (10) allows for the derivation of the switching field. The coercivity h_c follows from:

$$\frac{\partial \varepsilon_{\text{tot}}}{\partial m} = 0 \rightarrow h_c = -(\varepsilon^{\text{MD}} - \varepsilon^{\text{SD}}). \tag{11}$$

The stripe arrays remain in the single domain state until the external magnetic field is large enough to overcome the energy barrier.

To allow for the comparison of the domain model with the experimental data shown in Figs. 1 and 2, the α-MnAs phase fraction has to be correlated with the temperature. Here, the ratio of the respective saturation magnetizations at given temperatures and at $T=0$ °C is used to determine $\phi_\alpha(T)$. It has to be noted that this approach introduces a small systematic error since the magnetic moment decreases with temperature too.

Figure 7 compares the experimental data with the results obtained from the domain model [Eq. (11)]. Both the absolute values of the coercivity, as well as their dependence on the α-phase fraction, are in excellent agreement. The calculated coercive field values are slightly larger than the experimental values and the maximum of the coercive field is shifted toward larger α-MnAs phase fractions. The main reason is the influence of the stripe period p. A larger stripe period would shift the curve toward a lower α-MnAs fractions. It also lowers the energy difference $\varepsilon^{\text{MD}}-\varepsilon^{\text{SD}}$, leading to a decrease in the calculated coercivity.

Another remarkable feature in the coercive field curve is the anomalous increase in the coercivity for very small α-MnAs phase fractions (experimental data in Fig. 7). The lower boundary of the applicability of the domain model is reached at $\phi_\alpha \approx 0.22$. The width of the stripes w_α becomes smaller than the film thickness and the shape anisotropy favors the out-of-plane direction (z axis) as the easy axis for higher temperatures. Consequently, the hysteresis curves measured along the in-plane a axis change their character from easy axis to hard axis (not shown), accompanied by an increase in coercivity. For higher temperatures very close to the phase transition, the α-phase pattern breaks down and small ferromagnetic particles remain in the β-MnAs matrix (shown by temperature-dependent MFM measurements; cf. Ref. 25). Again, the lateral dimensions of these particles are smaller than the film thickness and their easy axis will be in the out-of-plane direction.

Taking a closer look at the experimental hysteresis curves shown in Fig. 1 and their characteristics (Fig. 2), two minor features remain unexplained. First, although predicted by the domain model, the magnetization does not completely switch at once. A small fraction ($\lesssim 1\%$) remains which can be attributed to pinning centers that hinder the magnetic domains to switch. Moreover, the real stripe structure will most certainly deviate from the average stripe width assumed in the model. Edge dislocation defects in the stripe array, as well as fluctuation of the local stripe width, are observed experimentally and are not taken into account in the model. However, the fraction of the pinned parts of the film is small which indicates the local nature of this phenomenon.

A second more obvious feature is the rounding of the hysteresis curves near the coercive field. The rounding effect, which is more pronounced for higher temperatures, originates from the formation of edge domains. In the real stripes, the magnetization patterns of the domains deviate from the assumed primary magnetization direction (along the y axis) near the stripe edges. The normal component of the magnetization is decreased and thus the demagnetization energy. In the cross section of the stripe (y-z plane), the real magnetization pattern corresponds to the flower-state or the C and S states. They are known from thin-film soft magnetic material structures with submicron dimensions and are already reported to exist in MnAs thin films.[10,11] These edge domains can be considered as the onset of the formation of flux closure domains. However, the small thickness of the thin film prevents the formation of flux closure domains in depth, e.g., "Landau," type (II) and type (III) domains, i.e., a "short circuit" of the magnetic flux in the depth of the film—as known from thicker films (≥ 100 nm)—is excluded. Micromagnetic simulations reveal that the volume of the edge domains is constant (not shown). For smaller α-MnAs phase fractions and thus smaller stripe widths w_α (higher temperatures), edge domains contribute more, leading to an increased rounding of the magnetization curves, which conforms with the experimental finding (cf. Fig. 1).

V. CONCLUSIONS

In this paper a simple yet realistic model was employed to unveil the magnetization reversal of thin MnAs films on GaAs(001) in the phase coexistence regime. It is capable to correctly predict the magnetic properties of the stripe structure for a 60-nm-thick film. It has been found that interstripe coupling dominates the stripe array for large α-MnAs phase fractions in the absence of an applied magnetic field. The transition to a decoupled stripe array is sharp and takes place at an α-MnAs phase fraction of 0.81.

In the presence of an applied magnetic field, decoupled stripe arrays with an α-MnAs phase fraction between $0.74 \leq \phi_\alpha \leq 0.79$ change to interstripe coupled stripe arrays. It is concluded that depending on temperature and applied field, the stripe array can change its coupling state.

Independent of temperature, the saturation state is the magnetization state with minimum energy. Once the stripe array is in saturation, the magnetization reversal is governed by an interstripe coupled reversal mechanism. The coercive field of the global reversal was shown to be determined by the energy difference of the multidomain state with zero net magnetization and the single domain state of the stripe array, which is in excellent agreement with reported experimental findings.

ACKNOWLEDGMENTS

The authors want to thank the Federal Ministry of Education and Research (BMBF) of the Federal Republic of Germany and the Natural Sciences and Engineering Research Council of Canada (NSERC) for partial financial support and K. H. Ploog for his continuous and generous support. R.E.-H. gratefully acknowledges financial support from the Alexander-von-Humboldt Foundation.

*rengelhe@mrl.ucsb.edu

[1] S. P. Li, W. S. Lew, J. A. C. Bland, L. Lopez-Diaz, M. Natali, C. A. F. Vaz, and Y. Chen, Nature (London) **415**, 600 (2002).
[2] O. Fruchart and A. Thiaville, C. R. Phys. **6**, 921 (2005).
[3] E. Y. Vedmedenko, N. Mikuszeit, H. P. Oepen, and R. Wiesendanger, Phys. Rev. Lett. **95**, 207202 (2005).
[4] K. Nielsch, R. Wehrspohn, J. Barthel, J. Kirschner, U. Gösele, S. Fischer, and H. Kronmüller, Appl. Phys. Lett. **79**, 1360 (2001).
[5] J. I. Martín, J. Nogués, K. Liu, J. L. Vicent, and I. K. Schuller, J. Magn. Magn. Mater. **256**, 449 (2003).
[6] O. Henkel, Phys. Status Solidi **17**, K99 (1966).
[7] O. Fruchart, J.-P. Nozières, W. Wernsdorfer, D. Givord, F. Rousseaux, and D. Decanini, Phys. Rev. Lett. **82**, 1305 (1999).
[8] L. Däweritz, Rep. Prog. Phys. **69**, 2581 (2006).
[9] It is still under discussion whether β-MnAs is paramagnetic or antiferromagnetic with a lack of long-range order. For a discussion see H. Yamaguchi, A. K. Das, A. Ney, T. Hesjedal, C. Pampuch, D. M. Schaadt, and R. Koch, Europhys. Lett. **72**, 479 (2005); Manish K. Niranjan, B. R. Sahu, and Leonard Kleinman, Phys. Rev. B **70**, 180406(R) (2004).
[10] R. Engel-Herbert, T. Hesjedal, and D. M. Schaadt, J. Appl. Phys. **101**, 09K103 (2007).
[11] R. Engel-Herbert, T. Hesjedal, J. Mohanty, D. M. Schaadt, and K. H. Ploog, Phys. Rev. B **73**, 104441 (2006).
[12] R. Engel-Herbert, T. Hesjedal, and D. M. Schaadt, Phys. Rev. B **75**, 094430 (2007).
[13] R. Engel-Herbert, A. Locatelli, S. Cherifi, D. M. Schaadt, J. Mohanty, L. Däweritz, K. H. Ploog, E. Bauer, R. Belkhou, S. Heun, A. Pavlovska, and T. Hesjedal, Appl. Phys. A: Mater. Sci. Process. **84**, 231 (2006).
[14] R. Engel-Herbert, T. Hesjedal, J. Mohanty, D. M. Schaadt, and K. H. Ploog, Phys. Rev. B **73**, 104441 (2006).
[15] A. Ney, T. Hesjedal, C. Pampuch, A. K. Das, L. Däweritz, R. Koch, K. H. Ploog, T. Tolinski, J. Lindner, K. Lenz, and K. Baberschke, Phys. Rev. B **69**, 081306(R) (2004).
[16] R. Engel-Herbert and T. Hesjedal (unpublished).
[17] H. J. G. Draaisma and W. J. M. de Jonge, J. Appl. Phys. **62**, 3318 (1987).
[18] M. Tanaka, J. P. Harbison, T. Sands, T. L. Cheeks, V. G. Keramidas, and G. M. Rothberg, J. Vac. Sci. Technol. B **12**, 1091 (1994).
[19] M. Tanaka, Physica E (Amsterdam) **2**, 372 (1998).
[20] F. Schippan, A. Trampert, L. Däweritz, and K. H. Ploog, J. Vac. Sci. Technol. B **17**, 1716 (1999).
[21] F. Schippan, M. Kästner, L. Däweritz, and K. H. Ploog, Appl. Phys. Lett. **76**, 834 (2000).
[22] A. Ney, T. Hesjedal, C. Pampuch, J. Mohanty, A. K. Das, R. Koch, L. Däweritz, and K. H. Ploog, Appl. Phys. Lett. **83**, 2850 (2003).
[23] R. Zdyb, A. Locatelli, S. Heun, S. Cherifi, R. Belkhou, and E. Bauer, Surf. Interface Anal. **37**, 239 (2005).
[24] R. Magalhaes-Paniago, L. N. Coelho, B. R. A. Neves, H. Westfahl, F. Iikawa, L. Daweritz, C. Spezzani, and M. Sacchi, Appl. Phys. Lett. **86**, 053112 (2005).
[25] T. Plake, T. Hesjedal, M. Kästner, L. Däweritz, and K. H. Ploog, Appl. Phys. Lett. **82**, 2308 (2003).
[26] L. Däweritz, C. Herrmann, J. Mohanty, T. Hesjedal, K. H. Ploog, E. Bauer, A. Locatelli, S. Cherifi, R. Belkhou, A. Pavlovska, and S. Heun, J. Vac. Sci. Technol. B **23**, 1759 (2005).
[27] A. N. Bogdanov and U. K. Rößler, arXiv:cond-mat/0606671 (unpublished).
[28] R. Engel-Herbert, Ph.D. thesis, Humboldt-Universität, 2006.
[29] F. Schippan, G. Behme, L. Däweritz, K. H. Ploog, B. Dennis, K.-U. Neumann, and K. R. A. Ziebeck, J. Appl. Phys. **88**, 2766 (2000).
[30] L. B. Steren, J. Milano, V. Garcia, M. Marangolo, M. Eddrief, and V. H. Etgens, Phys. Rev. B **74**, 144402 (2006).
[31] K. H. Ploog, L. Däweritz, R. Engel-Herbert, and T. Hesjedal, Phys. Status Solidi A **203**, 3574 (2006).
[32] J. Kaczer and L. Murtinova, Phys. Status Solidi A **23**, 79 (1974).
[33] A. Hubert and R. Schäfer, *Micromagnetic Domains* (Springer, Berlin, 1998).
[34] A. Aharoni, J. Appl. Phys. **83**, 3432 (1998).